



DATABASE

m⁶A-TSHub: Unveiling the Context-specific m⁶A Methylation and m⁶A-affecting Mutations in 23 Human Tissues



Bowen Song^{1,2,3}, Daiyun Huang^{4,5,*}, Yuxin Zhang⁴, Zhen Wei^{4,6}, Jionglong Su⁷, João Pedro de Magalhães⁶, Daniel J. Rigden³, Jia Meng^{3,4,8}, Kunqi Chen^{1,*}

¹ Key Laboratory of Gastrointestinal Cancer (Fujian Medical University), Ministry of Education, School of Basic Medical Sciences, Fujian Medical University, Fuzhou 350004, China

² Department of Mathematical Sciences, Xi'an Jiaotong-Liverpool University, Suzhou 215123, China

³ Institute of Systems, Molecular and Integrative Biology, University of Liverpool, Liverpool L69 7ZB, United Kingdom

⁴ Department of Biological Sciences, Xi'an Jiaotong-Liverpool University, Suzhou 215123, China

⁵ Department of Computer Science, University of Liverpool, Liverpool L69 7ZB, United Kingdom

⁶ Institute of Ageing & Chronic Disease, University of Liverpool, Liverpool L69 7ZB, United Kingdom

⁷ School of AI and Advanced Computing, Xi'an Jiaotong-Liverpool University, Suzhou 215123, China

⁸ AI University Research Centre, Xi'an Jiaotong-Liverpool University, Suzhou 215123, China

Received 12 October 2021; revised 19 August 2022; accepted 2 September 2022

Available online 9 September 2022

Handled by Jianhua Yang

KEYWORDS

N⁶-methyladenosine;
Context-specific analysis;
Cancer mutation;
Genome analysis;
Functional annotation

Abstract As the most pervasive epigenetic marker present on mRNAs and long non-coding RNAs (lncRNAs), N⁶-methyladenosine (m⁶A) RNA methylation has been shown to participate in essential biological processes. Recent studies have revealed the distinct patterns of m⁶A methylome across human tissues, and a major challenge remains in elucidating the tissue-specific presence and circuitry of m⁶A methylation. We present here a comprehensive online platform, m⁶A-TSHub, for unveiling the context-specific m⁶A methylation and genetic mutations that potentially regulate m⁶A epigenetic mark. m⁶A-TSHub consists of four core components, including (1) m⁶A-TSDB, a comprehensive database of 184,554 functionally annotated m⁶A sites derived from 23 human tissues and 499,369 m⁶A sites from 25 tumor conditions, respectively; (2) m⁶A-TSFinder, a web server for high-accuracy prediction of m⁶A methylation sites within a specific tissue from RNA sequences, which was constructed using multi-instance deep neural networks with gated attention; (3) m⁶A-TSVar, a web server for assessing the impact of genetic variants on tissue-specific m⁶A RNA modifications; and (4) m⁶A-CAVar, a database of 587,983 The Cancer Genome Atlas (TCGA) cancer

* Corresponding authors.

E-mail: kunqi.chen@fjmu.edu.cn (Chen K), daiyun.huang@liverpool.ac.uk (Huang D).

Peer review under responsibility of Beijing Institute of Genomics, Chinese Academy of Sciences / China National Center for Bioinformation and Genetics Society of China.

<https://doi.org/10.1016/j.gpb.2022.09.001>

1672-0229 © 2023 The Authors. Published by Elsevier B.V. and Science Press on behalf of Beijing Institute of Genomics, Chinese Academy of Sciences / China National Center for Bioinformation and Genetics Society of China.

This is an open access article under the CC BY license (<http://creativecommons.org/licenses/by/4.0/>).

mutations (derived from 27 cancer types) that were predicted to affect m⁶A modifications in the primary tissue of cancers. The database should make a useful resource for studying the m⁶A methylome and the genetic factors of epitranscriptome disturbance in a specific tissue (or cancer type). m6A-TSHub is accessible at www.xjtlu.edu.cn/biologicalsciences/m6ats.

Introduction

Among the more than 150 distinct chemical modifications naturally decorating cellular RNAs [1], N⁶-methyladenosine (m⁶A) is the most pervasive marker on mRNAs and long non-coding RNAs (lncRNAs), and has been associated with a number of essential biological functions and processes [2,3], including mRNA stability [4], splicing [5], translation [6,7], heat shock [8], DNA damage [9], and embryonic development [10]. Increasing evidence has indicated a critical role of m⁶A dysregulation in various human diseases, especially multiple cancers, such as breast cancer [11,12] and prostate cancer [13]. For example, inhibition of an m⁶A methyltransferase (METTL3) could be used as a potential therapeutic strategy against acute myeloid leukemia [14].

Developed in 2012, m⁶A-seq (methylated RNA immunoprecipitation sequencing; MeRIP-seq) was the first whole transcriptome m⁶A profiling approach [15,16]. It relies on antibody-based enrichment of the m⁶A signals, enabling the identification of m⁶A-containing regions with a resolution of around 100 nt. Currently, m⁶A-seq is still the most popular m⁶A profiling approach and has been applied in more than 30 different organisms. Besides m⁶A-seq, recent advances in integration of ultraviolet cross-linking, enzymatic activity, and domain fusion have offered improved even base-resolution m⁶A detection through techniques such as, miCLIP/m⁶A-CLIP-seq [17,18], m⁶A-REF-seq [19], and DART-seq [20]. However, compared with m⁶A-seq, these approaches require more complicated experimental procedures and have therefore been applied in fewer biological contexts.

To date, more than 120 computational approaches have been developed for the computational identification of RNA modifications [21,22] from the primary RNA sequences. These include the iRNA toolkits [23–31], MultiRM [32], DeepPromise [22], RNAm5CPred [33], SRAMP [11], Gene2vec [34], PEA [35], PPUS [36], WHISTLE [37], m5UPred [38], WeakRM frameworks [39,40], m6ABoost [41], PULSE [42], m6AmPred [43], BERMP [44], and MASS [45]. Together, these efforts have greatly advanced our understanding of multiple RNA modifications in different RNA regions and in various species (see recent reviews [22,46–48]). A number of epitranscriptome databases have been constructed. MODOMICS collects the pathways related to more than 150 different RNA modifications [1]. RMBase [49], m⁵C-Atlas [50], and m⁶A-Atlas [51] assembled millions of experimentally validated m⁶A and m⁵C sites. REPIC has been established as a comprehensive atlas for exploring the association between m⁶A RNA methylation and chromatin modifications [52]. ConsRM provides the conservation score of individual m⁶A sites at the base resolution, which can be used to differentiate the functionally important and ‘passenger’ m⁶A sites [53]. m6A2Target compiles the target molecules of m⁶A methyltransferases, demethylases, and binding proteins [54]. This work has extended our knowledge of the functional epitranscriptome, and greatly facilitated relevant research. Special efforts have also been

made to explore the effects of genetic variants on RNA modifications and their association with various diseases. m6AVar [55] was the first database that focused on the genetic factors related to epitranscriptome disturbance. It documented more than 400,000 m⁶A-affecting genetic variants, which were further labeled with disease and phenotype associations identified from genome-wide association study (GWAS) analysis. This prediction framework was improved and later applied to eight other RNA modifications (m⁵C, m¹A, m⁵U, Ψ, m⁶Am, m⁷G, and 2'-O-Me, and A-to-I) by RMVar [56] and RMDisease [57]. These aforementioned databases systematically revealed the general association between epitranscriptome layer dysregulation and various diseases (see a recent review [58]).

Existing computational approaches for epitranscriptome analysis have been quite successful in providing a large quantity of useful information; however, most of them failed to consider the tissue specificity of m⁶A epi-transcriptome [59,60]. Indeed, a recent study by Liu et al. unveiled distinct tissue-specific signatures of the m⁶A epitranscriptome in human and mouse [61], which are induced by context-specific expression of m⁶A regulators [methyltransferases, demethylases, and RNA-binding proteins (RBPs)] [62] and genetic drivers [63]. Nevertheless, most existing approaches for RNA modification site prediction completely ignore the context specificity of the epitranscriptome and simply assume a single model for different tissues, undermining their accuracy and applicability. To the best of our knowledge, the only three approaches that clearly support the identification of tissue-specific m⁶A methylation are im6A-TS-CNN [64], iRNA-m6A [65], and TS-m6A-DL [66], all covering only three human tissue types (brain, liver, and heart). Similarly, when screening for the genetic variants that can affect RNA modifications, previous work assumes a consistent influence in different tissues (see Table S1 for a detailed description and comparison). However, because different epitranscriptome patterns were observed among different tissues, genetic mutations that can alter m⁶A methylation in one tissue may not necessarily function similarly in a different tissue. Likewise, there are significant differences in incidence, mortality, and molecular signatures across cancer originating from different tissues [67,68]. It is therefore highly desirable to develop approaches that could take full advantage of the tissue-specific RNA methylation profiles so as to make more reliable predictions with respect to a specific tissue type [69]. This is particularly critical for studying the epitranscriptome circuits of diseases that are explicitly associated with a specific tissue, such as, cancers.

To address this issue, we present here a comprehensive online platform m6A-TSHub for unveiling the context-specific m⁶A methylation and m⁶A-affecting mutations in 23 human tissues. m6A-TSHub consists of four core components: (1) m6A-TSDB, a database for 184,554 experimentally validated m⁶A-containing peaks (m⁶A sites) derived from 23 distinct human normal tissues and 499,369 m⁶A-containing peaks (m⁶A sites) from 25 matched tumor conditions,

extracted from 233 m⁶A-seq samples, respectively; (2) m6A-TSFinder, an integrated online server for the prediction of tissue-specific m⁶A modifications in 23 human tissues, built upon a gated attention-based multi-instance deep neural network; (3) m6A-TSVar, a web server for systemically assessing the tissue-specific impact of genetic variants on m⁶A RNA modification in 23 human tissues; (4) m6A-CAVar, a database of 587,983 The Cancer Genome Atlas (TCGA) cancer mutations (derived from 27 cancer types) that may lead to the gain or loss of m⁶A sites in the corresponding cancer-originating tissues.

In addition, the m⁶A-associated variants were also annotated with their potential post-transcriptional regulatory roles, including RBP binding regions, microRNA (miRNA) targets, and splicing sites, along with their known disease and phenotype linkage integrated from GWAS catalog [70] and ClinVar databases [71]. The m6A-TSHub is freely accessible at www.xjtlu.edu.cn/biologicalsciences/m6ats, and should be a useful resource for studying the m⁶A methylome and genetic basis of epitranscriptome disturbance with respect to a specific cancer type or tissue. The overall design of m6A-TSHub is shown in Figure 1.

Data collection and processing

Data resource — m6A-TSDB

We collected the epitranscriptome profiles of 23 healthy human tissues, from which the tissue-specific RNA methylation patterns were learned using deep neural networks. Specifically, the raw sequencing data of 78 m⁶A-seq samples were downloaded directly from Gene Expression Omnibus (GEO) repository of National Center for Biotechnology Information (NCBI) [72] and National Genomics Data Center (NGDC) [73] (Table S2). Adaptors and low-quality nucleotides were removed by Trim Galore [74], followed by quality control using FastQC. The processed reads were then aligned to the reference genome GRCh37/hg19 by HISAT2 [75]. The m⁶A-enriched regions (peaks) located on transcripts were detected by exomePeak2 [76] using its default setting with GC contents corrected. In total, m⁶A profiling samples from 23 healthy human tissues (184,554 m⁶A-containing peaks) were processed. We filtered all obtained m⁶A-enriched regions to retain peaks with at least one DRACH consensus motif and used these peak regions containing tissue-specific m⁶A signals as positive data. Negative data were randomly collected from non-peak regions located on the same transcript of the corresponding positive data, and cropped to balance the length and number between positive and negative regions (with a positive-to-negative ratio of 1:1). The genomic sequences of both positive and negative regions were then extracted for developing the tissue-specific m⁶A prediction model.

To evaluate the effect of cancer somatic variants on m⁶A methylation in their originating tissues, a total of 2,587,191 cancer somatic variants from 27 different cancer types were obtained from TCGA (release version v27.0-fix) [77] (Table S3). Meanwhile, 155 m⁶A-seq samples profiling the epitranscriptome (499,369 m⁶A-containing peaks) of 25 cancer cell lines (corresponding to 17 tissue types) were also obtained using the same data processing pipeline (Table S2), which were

used for the validation of the predicted effects on m⁶A methylation of the variants (detailed in the following).

Learning tissue-specific m⁶A methylation with deep neural networks — m6A-TSFinder

The purpose of weakly supervised learning is to develop predictive models by learning from weakly labeled data, such as m⁶A peaks of low resolution detected by the m⁶A-seq (or MeRIP-seq) technique [15,16]. Unlike supervised learning based on single-nucleotide resolution data, it works for the case in which only coarse-grained labels (indicating whether a genome bin contains an m⁶A site) are available for these peaks of various lengths. We previously proposed a general weakly supervised learning framework WeakRM [78], which takes labels at the sequence level (rather than a nucleotide level) as input and predicts the sub-regions that are most likely to contain the RNA modification. As a simplified illustration shown in Figure 2, the m6A-TSFinder framework is divided into several sub-sections. Firstly, multi-instance learning treats each entire RNA sequence as a ‘bag’, with multiple ‘instances’ within the ‘bag’ determined by a fixed-length sliding window. Previous studies have shown that a 40–50-nt context region is sufficient for modification predictions. Therefore, in m6A-TSFinder, a sliding window of 50 nt was used, which was also helpful in improving the prediction resolution. Secondly, the RNA instances were fed into the m6A-TSFinder model using one-hot encoding, which is widely used in deep learning-based models. The extracted instances pass through the same feature extraction module (the weights of the network are shared in this module) and output instance-level features. The network architecture of the feature extraction section used in m6A-TSFinder includes the first convolutional layer to capture motifs, a max-pooling layer to remove weak features and enlarge the receptive field, a dropout layer that prevents overfitting in training, and a second convolutional layer which learns local dependencies among motifs. In order to further improve the performance of the model, in m6A-TSFinder, we use a long short-term memory (LSTM) layer to replace the second convolutional layer, so that the model can learn the long-range dependence of the motif while maintaining local dependence. Lastly, gated attention was used as the score function to obtain bag-level probabilities from multiple instance-level features. The gated attention module consists of three fully connected layers. The first two layers learn hidden representations from the instance features using tanh and sigmoid activation functions. Their element-wise multiplication is then sent to the third fully connected layer, which learns the similarity between the product and a context feature vector and outputs an attention score for each instance. The score is further normalized using the softmax function, so that the weights of all instances add up to 1. The weighted summation of instance features is treated as the bag-level feature and used to output the final probability score. Together, our model can be trained end-to-end using the binary cross-entropy loss calculated by the bag-level label. Our model was trained using the Adam optimizer under the Tensorflow framework. The learning rate was initially set to 1E–4, and gradually decayed to 1E–5 during the training process of 20 epochs. It is worth mentioning that when the number of instances is consistently set to 1,

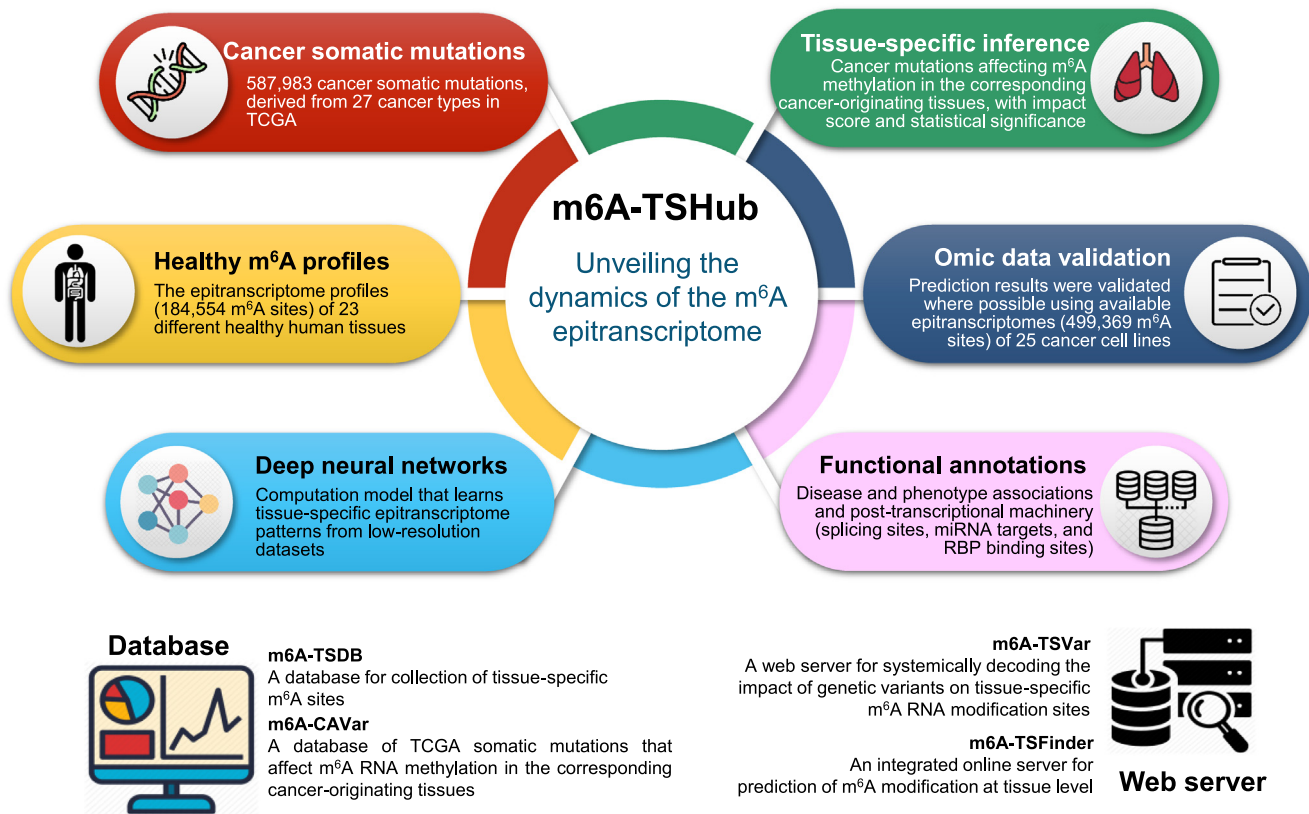


Figure 1 The overall design of m6A-TSHub

By integrating 184,554 m⁶A sites detected from 23 different healthy human tissues (m6A-TSDB), a deep learning framework that learns tissue-specific RNA methylation patterns was developed (m6A-TSFinder). The effect of genetic variants on tissue-specific m⁶A sites was then evaluated (m6A-TSVar). A total of 587,983 cancer somatic mutations were predicted to be able to affect m⁶A methylation of RNA in their corresponding cancer-originating tissues. The predicted m⁶A-affecting SNPs were then systematically validated using available cancer epitranscriptome datasets, and then functionally annotated with disease and phenotype associations from GWAS, along with features relating to the post-transcriptional machinery (miRNA target sites, splicing sites, and RBP binding sites) that are potentially mediated by m⁶A modification (m6A-CAVar). A web interface was constructed to enable the exploration, query, online analysis, and download of relevant results and data. m⁶A, N⁶-methyladenosine; TCGA, The Cancer Genome Atlas; GWAS, genome-wide association study; RBP, RNA-binding protein; miRNA, microRNA.

the weight of the instance is always 1, and the label becomes the instance level. In that case, the gated attention module is degraded, and the network becomes a strong supervised learning framework with two feature extraction layers.

Decoding the tissue-specific effect of variants on m⁶A methylation — m6A-TSVar & m6A-CAVar

Similar to previous studies [55,56,79,80], a cancer somatic variant is defined as a tissue-specific m⁶A variant if it could lead to the gain or loss of m⁶A methylation in a specific tissue. The tissue-specific inference was made possible by our deep neural network model m6A-TSFinder. Specifically, the predicted tissue-specific m⁶A variants were further classified into three confidence levels — low, medium, and high (Figure 3).

Low confidence level

An m⁶A-associated variant with a low confidence level was defined directly by the tissue-specific prediction model. For example, a synonymous somatic variant (Chr5: 92929473, positive strand, C > T, TCGA barcode:

TCGA-49-6742-01A-11D-1855-08) was extracted from The Cancer Genome Atlas Lung Adenocarcinoma (TCGA-LUAD) project, which was then predicted to eliminate the methylation of an experimentally validated m⁶A-containing region (Chr5:92929314-92929786, positive strand) originally detected in human lung tissue [61].

Medium confidence level

The m⁶A variants with a medium confidence level are those that can be verified on available epitranscriptome data from cancer samples originating from the matched tissue. After the low confidence level mentioned above, by checking the m⁶A-containing regions reported in lung adenocarcinoma cancer cell lines A549 [81] and H1299 [82], we confirmed that no m⁶A peaks were further observed in A549 and H1299 for the variant-affected region (Chr5:112176059-112176334, positive strand). Consequently, this LUAD somatic variant was upgraded to a 'medium' confidence level in the m6A-CAVar database. It is worth noting that the predicted m⁶A dynamics in m6A-CAVar were systematically validated using available epitranscriptome datasets from the matched healthy and

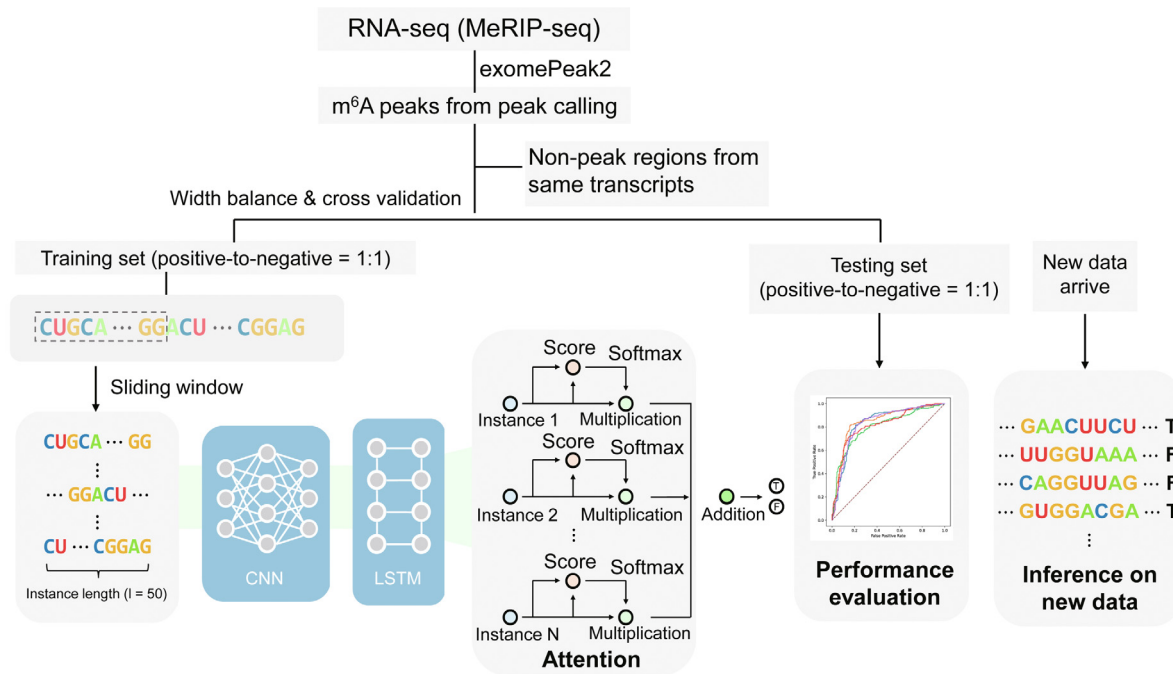


Figure 2 A simplified graphic illustration of the proposed m⁶A-TSFinder framework

RNA-seq, RNA sequencing; MeRIP-seq, methylated RNA immunoprecipitation sequencing; CNN, convolutional neural network; LSTM, long short-term memory.

cancer samples, providing another layer of quality assurance from real omic datasets: existing approaches only use those datasets to provide the m⁶A site information without searching for potential evidence of m⁶A status switching.

High confidence level

Only a very small number of variants have been clearly associated with diseases and phenotypes unveiled by GWAS analysis, and are known as disease-TagSNPs. These variants exhibited their clinical significance and are very likely to be functionally important. Thus, m⁶A variants of ‘high’ confidence level were defined as the validated m⁶A variants that can also be mapped to disease-TagSNPs extracted from ClinVar [71] and GWAS catalog [70], while those not validated were referred to as ‘critical’.

Additionally, the association level (AL) between an SNP and m⁶A RNA modification was defined as follows:

$$AL = \begin{cases} 2P_{SNP} - 2 \max(0.5, P_{WT}) & \text{for gain} \\ 2P_{WT} - 2 \max(0.5, P_{SNP}) & \text{for loss} \end{cases} \quad (1)$$

where P_{WT} and P_{SNP} represent the probability of m⁶A RNA modification for the wild-type and mutated sequences, respectively. The AL ranges from 0 to 1, with 1 indicating the maximum impact on m⁶A methylation. The statistical significance was assessed by comparing the ALs of all mutations, with which the upper bound of the P value can be calculated from its absolute ranking. The m⁶A-associated variants with $AL > 0.4$ and $P < 0.1$ were retained. We also considered the possibility of a variant destroying a part of (but not an entire) m⁶A peaks. For peaks wider than 500 nt, the impacts were also evaluated on the 200-nt flanking regions of the variant.

The predicted m⁶A variants were then validated on the epi-transcriptome datasets from the matched healthy and cancer

samples. We consider a prediction validated by omic data if the matched dynamics of m⁶A sites were observed under the healthy tissue and the cancer samples with the same tissue origin. It may be worth noting that, omic data were only used to inform the prediction of m⁶A sites in previous studies [55,56,79,80]; however, our analysis also relies on it to confirm the predicted disturbance of m⁶A status between the healthy and cancer conditions. This extra layer of confirmation directly from available omic datasets should effectively enhance the reliability of our database.

Functional annotation

The identified m⁶A variants were annotated with various information, including transcript region [coding sequence, 3' untranslated region (UTR), 5' UTR, start codon, and stop codon], gene annotation (gene symbol, gene type, and Ensembl gene ID), evolutionary conservation (phastCons 60-way), deleterious level by SIFT [83], PolyPhen2 HVAR [84], PolyPhen2HDIV [84], LRT [85] and FATHMM [86] using the ANNOVAR package [87], absolute ranking by comparing with the ALs of all mutations (top 1% and top 5%), and TCGA sample information (TCGA case ID, TCGA barcode, TCGA sample count, and sample total variant number). A total of 177,998 high-confidence m⁶A sites detected using base-resolution technology previously were collected and used to pinpoint the precise location of the mediated m⁶A sites within the variant-affected regions (Table S4). In addition, aspects of the post-transcriptional machinery that can be mediated by m⁶A methylation were also annotated, including RBP binding regions from POSTAR2 [88], miRNA-RNA interaction from miRanda [89] and starBase2 [90], and splicing sites from UCSC [91] annotation with GT-AG role. Furthermore,

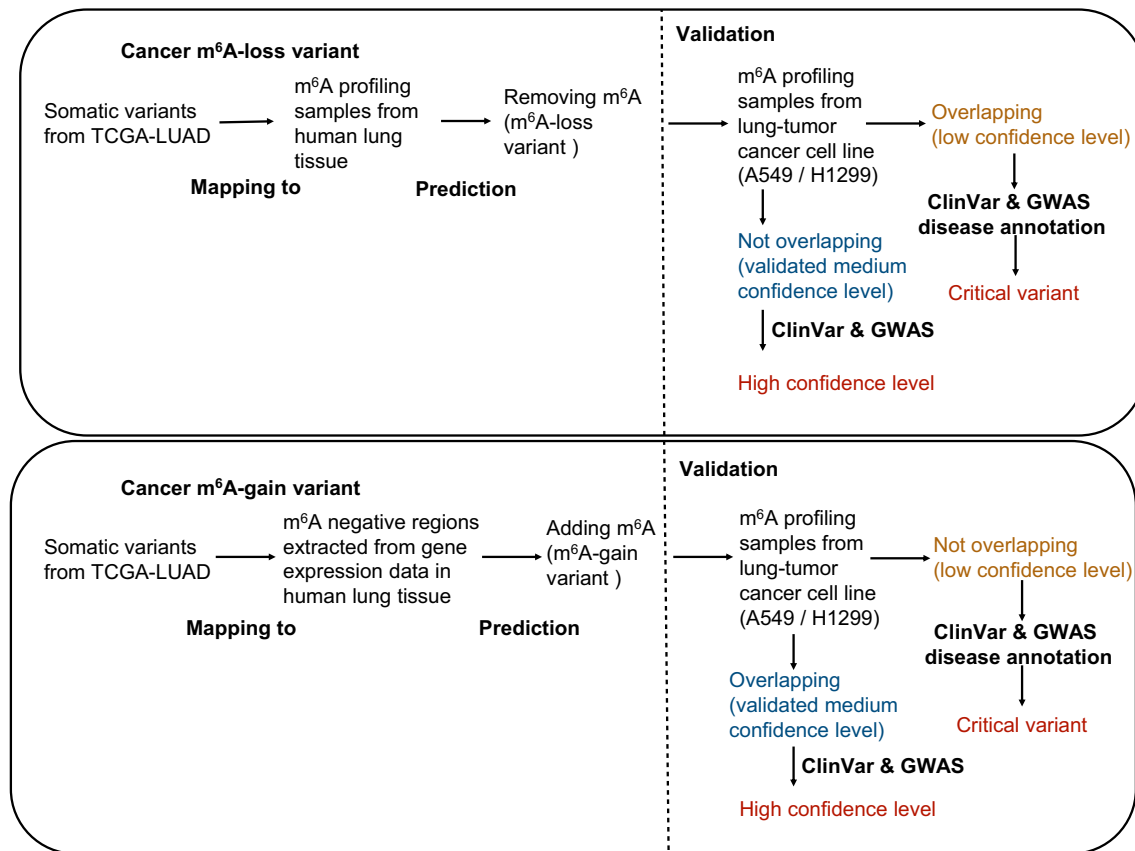


Figure 3 Workflow of how to determine the confidence level of m⁶A variants

Three types of confidence levels were applied. The cancer-driving somatic variants were extracted from TCGA projects, and mapped to the m⁶A profiling samples derived from corresponding tumor-growth tissues. A tissue-specific weakly supervised model was then applied to obtain m⁶A-associated variants classified into the low-confidence level group. m⁶A profiling samples from tumor-growth tissues were then used for validation of the prediction results, and the validated portion was classified into the medium-confidence level group. Lastly, all variants with a medium confidence level were annotated with disease information from ClinVar and GWAS, and then classified into the high-confidence level group. Lung tissue, healthy and cancerous, is used as an example here. The same protocol was followed for all 23 tissues. GWAS, genome-wide association study.

to unveil potentially related pathogenesis, any association between disease and m⁶A variants was extracted from the GWAS catalog [70] and ClinVar [71] databases.

Database and web interface implementation

Hypertext markup language (HTML), cascading style sheets (CSS), and hypertext preprocessor (PHP) were applied to construct the m6A-TSHub web interface. All metadata were stored using MySQL tables. Besides, ECharts was exploited to present statistical diagrams, and the Jbrowse genome browser [92] was included for interactive exploration and visualization of relevant records for genome regions of interest.

Database content and usage

Collection of m⁶A sites from 23 normal human tissues and 25 cancer cell lines in m6A-TSDB

In m6A-TSDB, a total of 184,554 and 499,369 m⁶A-containing peaks were collected from 23 normal human tissues and 25 cancer samples, respectively. Among them, 17 out of 25 tumor

samples have the m⁶A profiles of their matched primary tissues. The m⁶A-enriched peaks were called using exomePeak2 [76] with GC-correction function after mapping the processed reads to human reference genome version hg19. It is worth mentioning that, for a more complete m⁶A epitranscriptome landscape view, a total of 177,998 base-resolution m⁶A sites collected from 27 datasets using six different m⁶A profiling techniques were integrated and used to pinpoint the precise location of the mediated m⁶A sites within all tissue-specific m⁶A peaks (Table S4). In addition, all m⁶A-containing peaks were labeled with information showing whether these sites were affected by cancer somatic variants and potential involved post-transcriptional regulations. All data collected in the m6A-TSDB can be freely downloaded or shared.

Performance evaluation and model interpretation of tissue-specific m⁶A site prediction by m6A-TSFinder

The performance of tissue-specific m⁶A site predictors was evaluated using 10-fold cross-validation and independent testing. For each distinct human tissue, we randomly selected 15% of experimentally validated m⁶A sites and used them as an independent testing dataset. For 10-fold cross-validation, the

training data were randomly divided into 10 groups with the same number of positive and negative peaks. The prediction performance of each tissue-specific predictor is shown in **Table 1**. In general, the prediction accuracy for most tissues (20 out of the total 23 tissues) is in line with conventional approaches for m⁶A site prediction under strong supervision with base-resolution datasets, which typically reported a prediction performance between 0.8 and 0.85 in terms of the area under receiver operating characteristic (ROC) curve (AUROC) [22,93]. The performance for kidney (AUROC = 0.718), bone marrow (AUROC = 0.757), and brainstem (AUROC = 0.789) was somewhat worse, but the reasons are not very clear. In addition, in order to find the recurring sequence patterns preferred by each tissue-specific m⁶A prediction model, we further divided the peaks into instances of length (l = 50) and extracted the consensus motifs from instances with predicted values higher than 0.5 using integrated gradient and TF-Modisco, under each tissue model, respectively. By trimming the overall letter frequencies with three gaps and two mismatches allowed, we identified one consistency motif under all tissue models (Figure S1), which was matched to the known m⁶A consensus motif DRACH. Please refer to Figure S1 for details.

Performance compared with existing approaches

We further compared the performance of the proposed m6A-TSFinder with existing m⁶A predictors specifically targeted at the tissue level. Dao et al. previously developed a Support Vector Machine (SVM)-based model (iRNA-m6A) for m⁶A identification in the human brain, liver, and kidney [65]. Later, im6A-TS-CNN [64] and TS-m6A-DL [66] further improved prediction performance by applying a convolutional neural

network (CNN), using the same training and testing datasets provided in Dao's work. It is worth mentioning that the training and testing datasets used in their work contain positive and negative sequences fixed to 41-nt length with m⁶A sites or unmethylated adenosines in the center. These models learn to capture discriminative sequence patterns at positions with a fixed distance from the target adenosine. When making predictions, the well-trained models take the centered adenosine and its surrounding sequences and return the probability that the central adenosine is methylated. When only low-resolution data are available, sequence lengths vary from 100 nt to hundreds, and methylation is not fixed at the center of the sequence. Therefore, the pre-set requirements of these base-resolution models (TS-m6A-DL, im6A-TS-CNN, and iRNA-m6A) cannot be fulfilled, making it difficult to fairly evaluate their performance on low-resolution data. Furthermore, the only three tissue-specific base-resolution datasets originate from m6A-REF-seq, which can only detect m⁶A in NNACA, whereas the 23 low-resolution considered in this work contain m⁶A from broader sequence contexts. Inconsistencies between data further limit direct comparisons between models. Nevertheless, we apply m6A-TSFinder to the same training and testing datasets of the three base-resolution models to show performance and fair comparisons when base-resolution data are available. Specifically, as described in the “Data collection and processing” section, the prediction of m⁶A from fixed-length sequences centered at the target site can be considered a special case of m6A-TSFinder, in which each input sequence is treated as a single instance. As shown in **Table 2**, when tested on the independent dataset, m6A-TSFinder outperformed the three competing methods in two of the three tissues tested (brain and liver) and achieved the best average performance (AUROC = 0.8593). The improvement may be due to the

Table 1 Performance evaluation of tissue-specific m⁶A model

Tissue type	10-fold cross-validation				Independent testing			
	Accuracy	Precision	MCC	AUROC	Accuracy	Precision	MCC	AUROC
Lung	0.764	0.835	0.536	0.843	0.775	0.761	0.55	0.853
Bladder	0.758	0.760	0.517	0.836	0.766	0.750	0.532	0.848
Colon	0.740	0.770	0.482	0.810	0.744	0.730	0.490	0.810
Lymph node	0.771	0.797	0.544	0.844	0.78	0.735	0.570	0.844
Cerebrum	0.745	0.799	0.495	0.827	0.758	0.768	0.515	0.834
Cerebellum	0.715	0.718	0.432	0.798	0.72	0.731	0.441	0.801
Hypothalamus	0.733	0.724	0.467	0.799	0.746	0.74	0.493	0.811
Brainstem	0.727	0.742	0.454	0.764	0.721	0.713	0.443	0.789
Kidney	0.685	0.694	0.369	0.755	0.647	0.628	0.297	0.718
Bone marrow	0.694	0.634	0.391	0.757	0.698	0.721	0.397	0.757
Liver	0.742	0.747	0.484	0.805	0.737	0.717	0.476	0.803
Ovary	0.730	0.710	0.464	0.814	0.726	0.722	0.453	0.812
Prostate	0.752	0.779	0.507	0.819	0.759	0.736	0.521	0.830
Soft tissue	0.766	0.855	0.544	0.855	0.771	0.775	0.543	0.858
Skin	0.750	0.850	0.511	0.835	0.773	0.753	0.547	0.857
Stomach	0.772	0.820	0.549	0.852	0.77	0.764	0.539	0.848
Corpus uterus	0.722	0.656	0.452	0.813	0.734	0.715	0.470	0.822
Adrenal gland	0.737	0.771	0.474	0.804	0.741	0.716	0.485	0.817
Heart	0.778	0.824	0.558	0.854	0.772	0.759	0.546	0.846
Rectum	0.747	0.725	0.496	0.826	0.767	0.747	0.536	0.828
Testis	0.743	0.770	0.489	0.810	0.731	0.734	0.463	0.804
Thyroid gland	0.765	0.805	0.533	0.845	0.753	0.733	0.509	0.830
Pancreas	0.761	0.770	0.523	0.838	0.751	0.739	0.502	0.834

Note: MCC, Matthew's correlation coefficient; AUROC, the area under receiver operating characteristic curve.

application of the LSTM layer after the convolutional layer, which enables the model to learn the long-range dependencies between the motifs. In addition, by learning from the low-resolution datasets, we expanded the human tissues supported from 3 to 23, which could significantly facilitate future research focusing on the dynamics of m⁶A methylome across different tissues.

Assessing the impact of genetic variants on tissue-specific m⁶A sites by m6A-TSVar

The m6A-TSVar web server was designed to assess the impact of genetic variants on tissue-specific m⁶A RNA methylation using deep neural networks. The collected experimentally validated m⁶A peaks from 23 human tissues were integrated. The changes in the probability of m⁶A methylation affected by mutations were calculated, with the returned value of AL indicating how extreme the impact on m⁶A methylation was. To our best knowledge, the m6A-TSVar is the first web server for exploring m⁶A-affecting variants within a specific tissue by integrating the tissue-specific m⁶A patterns.

Screening for cancer variants that affect m⁶A in their primary tissues in m6A-CAVar

In m6A-CAVar, the cancer somatic variants from 27 TCGA projects were extracted. Their impacts on m⁶A RNA modifications in the corresponding 23 healthy human tissues were evaluated and then systematically validated using 17 paired normal and tumor samples. A total of 587,983 cancer somatic variants were predicted to affect the m⁶A methylation status in their originating tissues (the “low-confidence level” group). Among them, the dynamic m⁶A status induced by 122,473 variants was observed on the available epitranscriptome profiles (the “medium-confidence level” group), and 1718 confirmed m⁶A-variants were known to be associated with diseases and other phenotypes from GWAS analysis (the “high-confidence level” group) (Table 3). Please refer to “Data collection and processing” section for more details related to the definition of different confidence groups.

Deciphering the tissue specificity of cancer m⁶A variants

Of interest is whether m⁶A variants function in different cancer-originating tissues. For this purpose, we calculated the proportion of m⁶A variants that function in different numbers of tissues, and the results suggested that most m⁶A-associated cancer variants are tissue- and cancer-specific (93.25%), whereas only around 1.17% are functional in the

originating tissues of more than three types of cancers (Figure 4A). The consistency is much higher at the gene level. Only around 16.59% of m⁶A variant-carrying genes are associated with a single tissue. More than 60.29% were shared in more than three tissue types (Figure 4B), suggesting some common epitranscriptome layer circuitry at the gene level in different cancers. We further examined the proportion of shared m⁶A variant-carrying genes between two different tissues. As shown in Figure 4C, most tissues, e.g., skin and stomach, strongly correlated with each other. However, tissues like the heart, testis, and thyroid showed a rather weak association with other tissues, which may suggest more tissue-specific epitranscriptome circuitry for cancers originating in those tissues.

We finally identified the m⁶A variant-carrying genes that are associated with the most TCGA cancer types. Only experimentally validated m⁶A variants (medium confidence level and above) were considered here for a more reliable analysis. Top of the list was *CENPF*, in which variants may change its m⁶A methylation status in the primary tissue of 15 cancer types, followed by *DST*, *MKI67*, and *PLEC*, which were all related to 14 cancer types (detailed in Table S5). Among them, the roles in epitranscriptome regulation of *CENPF*, *MKI67*, and *PLEC* have been indicated previously in glioblastoma [94], breast cancer [95], and pancreatic cancer [96], respectively.

Enhanced web interface and application

The m6A-TSHub features a user-friendly web interface with multiple useful functions, including databases and online servers, which enable users to fast query databases, upload their own custom jobs, and download all m⁶A-related information at the tissue level. The collected functional m⁶A-affecting variants can be queried by a human body diagram according to their primary tissues (Figure 5A), as well as by different cancer types along with further filters (e.g., gene type, m⁶A status, confidence level, and disease association; Figure 5B). The query function also returns several categories of useful information, including TCGA project names [77], tumor-growth tissues, genes, chromosome regions, COSMIC ID [97], and disease phenotypes (Figure 5C). The details of tissue-specific m⁶A peaks collected in m6A-TSDB (Figure 5D) and cancer m⁶A-associated variants in m6A-CAVar (Figure 5E) can be viewed by clicking the site or variant ID, along with annotated disease-association regulations (Figure 5F). Furthermore, online servers allow for the identification of m⁶A sites and m⁶A-associated variants within user-defined regions, with 23 types of human tissues to be selected (Figure 5G and H). A genome browser is available for interactive exploration of the genome regions of interest, including the human gene

Table 2 Performance comparison between m6A-TSFinder and competing approaches on independent dataset

Tissue type	Performance on independent dataset (AUROC)			
	m6A-TSFinder	TS-m6A-DL	im6A-TS-CNN	iRNA-m6A
Brain	0.8132	0.8097	0.8056	0.7845
Liver	0.8850	0.8784	0.8805	0.8681
Kidney	0.8796	0.8802	0.8727	0.8565
Average	0.8593	0.8561	0.8529	0.8364

Note: For a fair comparison, the m6A-TSFinder was rebuilt for human brain, liver, and kidney, using the same training and testing datasets applied in the three previous studies. The 41-nt sequences were considered as one instance and fed into m6A-TSFinder.

Table 3 Tissue-specific m⁶A cancer variants collected in m6A-CAVar

Cancer type	Primary tissue	Matched cancer cell line	Variant type	Classification			Total	
				Low	Medium	High		
TCGA-LUAD	Lung	A549, H1299	Gain	27,845	6526	30	34,401	
TCGA-BLCA	Urinary bladder	BCa5637	Loss	1233	1391	2	2626	
			Gain	25,508	3702	13	29,223	
			Loss	3079	1691	6	4776	
TCGA-COAD	Colon	HT29, HCT116	Gain	30,540	8391	82	39,013	
TCGA-DLBC	B lymphocyte cell lines	OCI-Ly1	Loss	6	8284	74	8364	
			Gain	1189	82	2	1273	
			Loss	74	69	0	143	
TCGA-GBM	Cerebrum	U251, GOS-3, PBT003	Gain	8509	3648	47	12,204	
TCGA-GBM	Cerebellum	U251, GOS-3, PBT003	Loss	1453	1181	12	2646	
			Gain	8319	3659	38	12,016	
	Hypothalamus		Loss	1928	1271	4	3203	
			Gain	6723	3414	27	10,164	
	Brainstem		Loss	1522	1482	18	3022	
			Gain	7559	3168	40	10,767	
	TCGA-KIRC		Kidney	Loss	1374	1451	8	2833
				Gain	3844	227	4	4075
TCGA-LAML	HSCs	MOLM13, THP1, NOMO-1, MONO-MAC-6, MA9.3ITD	Loss	54	33	0	87	
			Gain	448	274	0	722	
			Loss	3	35	3	41	
TCGA-LIHC	Liver	HepG2, Huh7, SMMC7721, HCCLM3	Gain	7416	2511	2	9929	
TCGA-OV	Ovary	PEO1	Loss	18	1765	4	1787	
			Gain	7022	531	0	7553	
			Loss	1350	1090	6	2446	
TCGA-PRAD	Prostate gland	Cd-RWPE-1	Gain	3825	636	6	4467	
TCGA-SARC	Soft tissues	U20S	Loss	550	288	2	840	
			Gain	3592	1324	4	4920	
			Loss	373	28	0	401	
TCGA-SKCM	Skin	Mel624	Gain	79,470	17,177	118	96,765	
TCGA-STAD	Stomach	BGC823	Loss	6472	1559	2	8033	
			Gain	35,438	2202	34	37,674	
			Loss	1103	3313	27	4443	
TCGA-UCEC	Corpus uteri	HEC-1-A	Gain	80,712	38,242	266	119,220	
TCGA-LUSC	Lung	–	Loss	7813	1828	22	9663	
			Gain	31,106	–	118	31,224	
			Loss	2328	–	2	2330	
TCGA-MESO	Lung	–	Gain	595	–	4	599	
TCGA-LGG	Heart	–	Loss	57	–	0	57	
			Gain	674	–	5	679	
	Cerebrum		Loss	102	–	0	102	
			Gain	6714	–	92	6806	
	Cerebellum		Loss	1423	–	19	1442	
			Gain	6601	–	109	6710	
	Hypothalamus		Loss	1745	–	16	1761	
			Gain	5010	–	77	5087	
TCGA-KICH	Kidney	–	Loss	1698	–	11	1709	
			Gain	5740	–	114	5854	
	Kidney		Loss	1528	–	13	1541	
			Gain	484	–	9	493	
	Kidney		Loss	9	–	0	9	
			Gain	4028	–	17	4045	
	Liver		Loss	118	–	0	118	
			Gain	728	–	2	730	
TCGA-ACC	Adrenal gland	–	Loss	166	–	2	168	
TCGA-PCPG	Adrenal gland	–	Gain	2285	–	21	2306	
			Loss	385	–	3	388	
			Gain	345	–	1	346	
TCGA-READ	Rectum	–	Loss	57	–	0	57	
			Gain	12,433	–	100	12,533	
			Loss	1098	–	4	1102	
TCGA-THYM	Heart	–	Gain	520	–	7	527	
TCGA-THYM	Heart	–	Loss	80	–	2	82	

(continued on next page)

Table 3 (continued)

Cancer type	Primary tissue	Matched cancer cell line	Variant type	Classification			Total
				Low	Medium	High	
TCGA-TGCT	Testis	–	Gain	405	–	3	408
			Loss	109	–	0	109
TCGA-THCA	Thyroid gland	–	Gain	992	–	6	998
			Loss	156	–	0	156
TCGA-PAAD	Pancreas	–	Gain	6473	–	55	6528
			Loss	1236	–	3	1239
Total	–	–	–	463,792	122,473	1718	587,983

Note: TCGA-LUAD, The Cancer Genome Atlas Lung Adenocarcinoma; TCGA-BLCA, The Cancer Genome Atlas Bladder Urothelial Carcinoma; TCGA-COAD, The Cancer Genome Atlas Colon Adenocarcinoma; TCGA-DLBC, The Cancer Genome Atlas Lymphoid Neoplasm Diffuse Large B-cell Lymphoma; TCGA-GBM, The Cancer Genome Atlas Glioblastoma Multiforme; TCGA-KIRC, The Cancer Genome Atlas Kidney Renal Clear Cell Carcinoma; TCGA-LAML, The Cancer Genome Atlas Acute Myeloid Leukemia; TCGA-LIHC, The Cancer Genome Atlas Liver Hepatocellular Carcinoma; TCGA-OV, The Cancer Genome Atlas Ovarian Serous Cystadenocarcinoma; TCGA-PRAD, The Cancer Genome Atlas Prostate Adenocarcinoma; TCGA-SARC, The Cancer Genome Atlas Sarcoma; TCGA-SKCM, The Cancer Genome Atlas Skin Cutaneous Melanoma; TCGA-STAD, The Cancer Genome Atlas Stomach Adenocarcinoma; TCGA-UCEC, The Cancer Genome Atlas Uterine Corpus Endometrial Carcinoma; TCGA-LUSC, The Cancer Genome Atlas Lung Squamous Cell Carcinoma; TCGA-MESO, The Cancer Genome Atlas Mesothelioma; TCGA-LGG, The Cancer Genome Atlas Brain Lower Grade Glioma; TCGA-KICH, The Cancer Genome Atlas Kidney Chromophobe; TCGA-KIRP, The Cancer Genome Atlas Kidney Renal Papillary Cell Carcinoma; TCGA-CHOL, The Cancer Genome Atlas Cholangiocarcinoma; TCGA-ACC, The Cancer Genome Atlas Adrenocortical Carcinoma; TCGA-PCPG, The Cancer Genome Atlas Pheochromocytoma And Paraganglioma; TCGA-READ, The Cancer Genome Atlas Rectum Adenocarcinoma; TCGA-THYM, The Cancer Genome Atlas Thymoma; TCGA-TGCT, The Cancer Genome Atlas Testicular Germ Cell Tumors; TCGA-THCA, The Cancer Genome Atlas Thyroid carcinoma; TCGA-PAAD, The Cancer Genome Atlas Pancreatic Adenocarcinoma; HSC, hematopoietic stem cell.

annotation track, 23 normal tissue tracks, 25 cancer cell line tracks, single-base m⁶A epitranscriptome landscape track, and post-transcriptional regulation tracks. All metadata provided in the m6A-TSHub can be freely downloaded, along with server scripts provided to run the prediction tools locally (required language: R and Python). Users can refer to the ‘help’ and ‘download’ page for more detailed guidance and instructions.

Case study 1: *PIK3CA* variant in colon cancer

Previous studies have reported that m⁶A RNA modification plays an important role in colon cancer [61,98–100]. The Cancer Genome Atlas Colon Adenocarcinoma (TCGA-COAD) project [77] presented a large number of somatic variants identified from various colon adenocarcinoma samples. However, it is still unclear which single genetic variant may lead to m⁶A dysregulation. In m6A-CAVar, a somatic variant at Chr3:178952085 (A > T) on *PIK3CA* identified from TCGA-COAD project (TCGA barcode: TCGA-AA3821-01A-01W-0995-10) was predicted to erase the m⁶A methylation of a region (Chr3:178951888-178952363, positive strand). The m⁶A methylation was observed in healthy human colon, but disappeared in the colon adenocarcinoma cancer cell line HCT116 [101]. This somatic variant is also recorded in the COSMIC database from colon tumor samples under the legacy identifier of COSM776, and reported to be associated with 27 submitted interpretations and evidence in the ClinVar database [71], including *PIK3CA*-related overgrowth spectrum (ClinVar accession: RCV000201235.1), breast adenocarcinoma (ClinVar accession: RCV000014629.5), and pancreatic adenocarcinoma (ClinVar accession: RCV000417557.1). Taken together, these observations strongly support the functional importance of this variant. Additionally, the m⁶A-associated variant falls within the binding regions of two RBPs

(TARDBP and NUDT21), whose interaction may be regulated by the loss of m⁶A methylation in the cancer condition, providing some putative downstream regulatory consequences of the variant.

Case study 2: *PLEC* variant in glioblastoma

Glioblastoma (GBM) is the most aggressive type of brain tumor and is associated with rising mortality. The roles of m⁶A regulators in this disease have been previously indicated [102–105]. A somatic cancer variant on *PLEC* was identified from the The Cancer Genome Atlas Glioblastoma Multiforme (TCGA-GBM) project (TCGA barcode: TCGA-06-5416-01A-01D-1486-08) at Chr8:144991388 (C > T). This cancer variant was predicted to lead to a gain of an m⁶A site on a previously unmethylated region in a healthy human cerebrum. Indeed, an m⁶A site was detected in this region from malignant GBM tumor cell line U-251. This mutation has a record in ClinVar database (ClinVar accession: RCV000177727.1). Screening for potential post-transcriptional regulations revealed that the cancer variant falls within the target binding regions of six RBPs, including the m⁶A reader YTHDF1, which is known to bind m⁶A-containing RNAs and promote cancer stem cell properties of GBM cells [106]. It should be of immediate interest to ask whether the methylation of *PLEC* regulates its interaction with YTHDF1 and other RBPs, and what the functional consequences are.

Case study 3: *EGFR* variant in lung cancer

The associations between m⁶A RNA modifications and human lung cancers have been well studied. The m⁶A eraser FTO may be a prognostic factor in The Cancer Genome Atlas Lung Squamous Cell Carcinoma (TCGA-LUSC) [107], and the

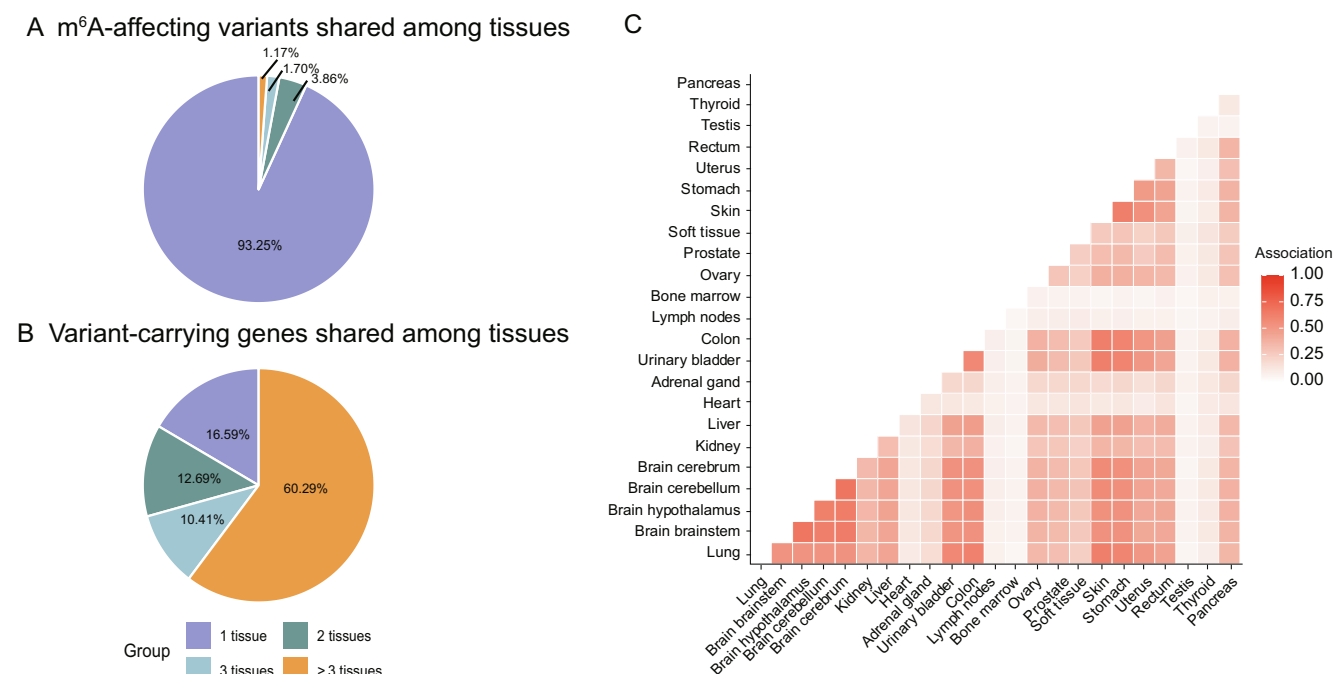


Figure 4 Tissue specificity of cancer m⁶A variants

A. The proportion of m⁶A variants that are shared among different tissues. Most m⁶A-associated variants (93.25%) were identified in only 1 tissue, with 3.86%, 1.70%, and 1.17% identified in 2, 3, and more than 3 tissues, respectively. **B.** The proportion of m⁶A variant-carrying genes shared among tissues. The consistency is much higher at the gene level. Most m⁶A variant-carrying genes are shared among multiple tissues, with only 16.59% associated to one tissue type. **C.** The pairwise association of tissues in terms of proportion of shared m⁶A variant-carrying genes. Most tissues are significantly correlated. The exceptions are heart, adrenal gland, lymph nodes, bone marrow, testis, and thyroid.

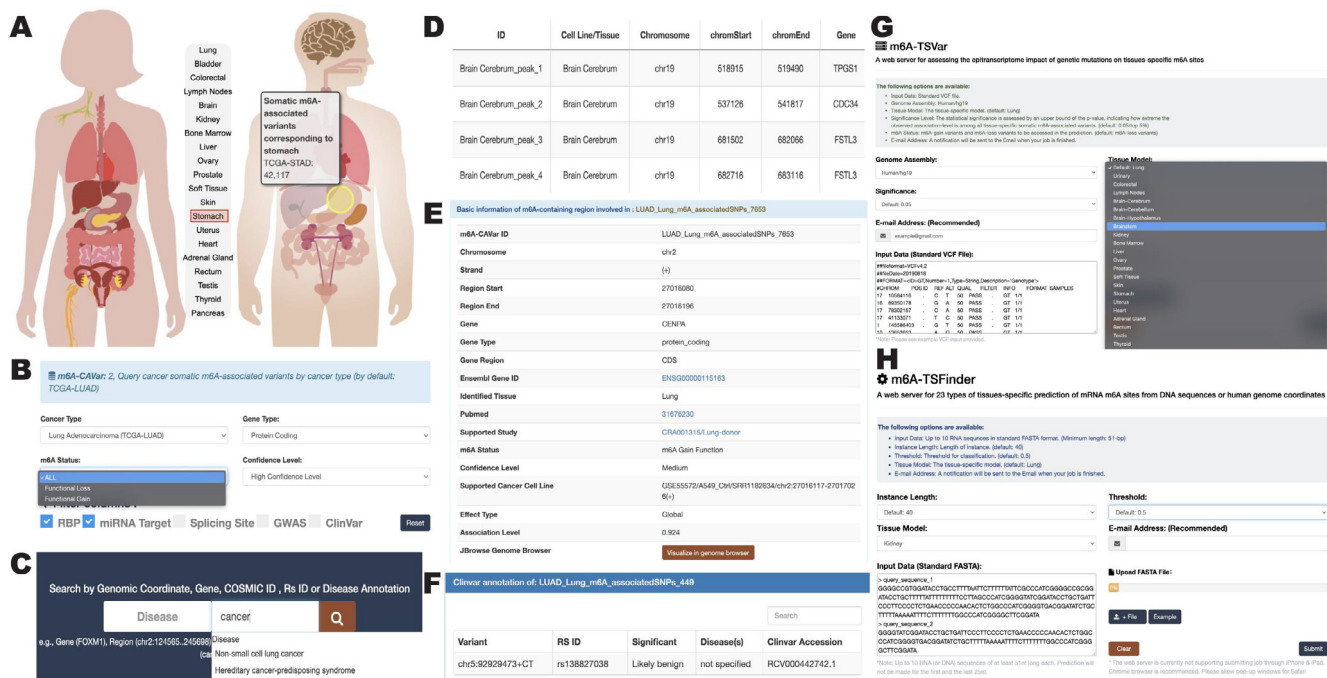


Figure 5 Enhanced web interface

A. A human body diagram is available for querying cancer somatic m⁶A-associated variants in their originating tissues. **B.** Users can query the associated variants by cancer type. **C.** Users can also query the variant-associated disease, region, gene symbol, COSMIC, and Rs ID, and further filter the returned results. **D.** Details of tissue-specific m⁶A peaks collected in m6A-TSDB. **E.** Details of cancer-related m⁶A-associated variants. **F.** Details of disease annotation involved. **G.** The online tools provided for analysis of user-uploaded files, including assessing m⁶A-associated variants in tissues (m6A-TSVar). **H.** The online tool for identifying tissue-specific m⁶A sites (m6A-TSFinder).

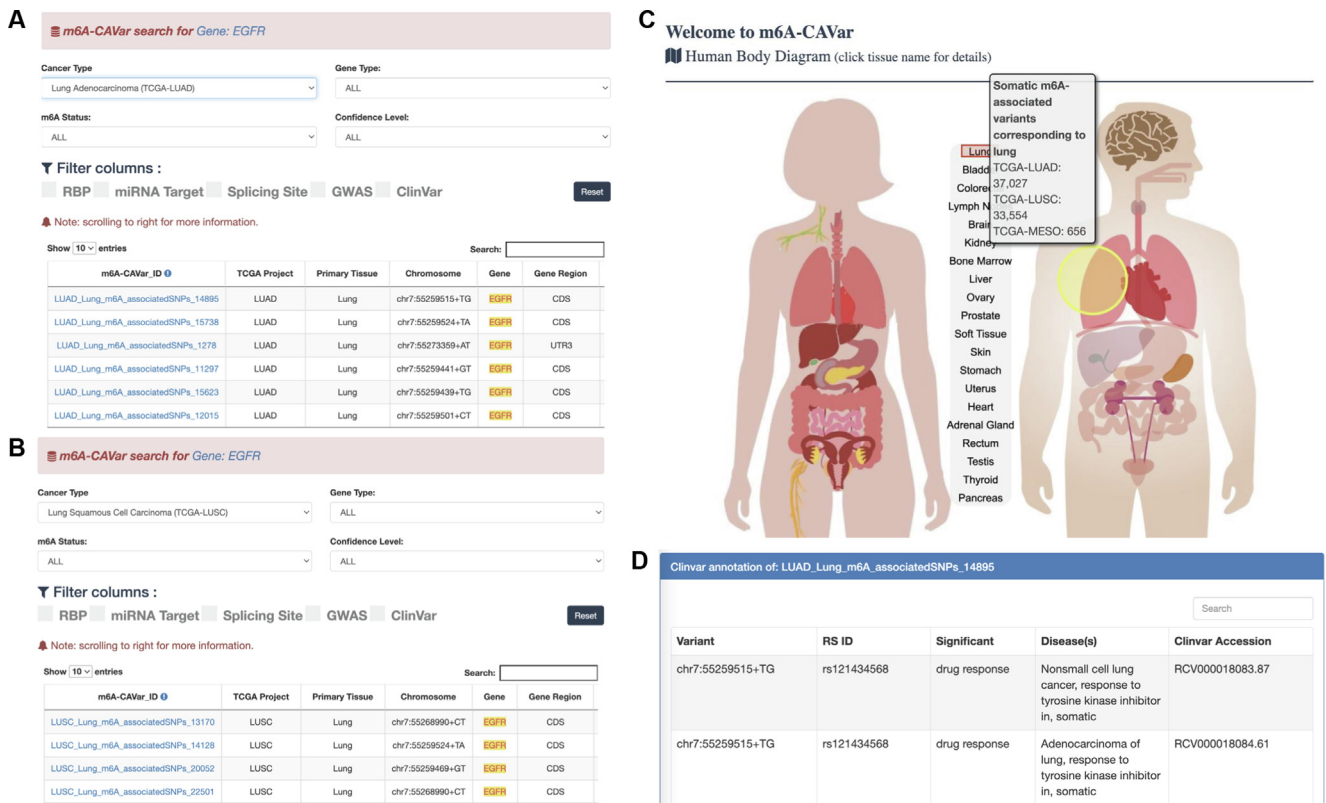


Figure 6 Case study on the *EGFR* gene

A. Searching for the gene '*EGFR*' in m6A-CAVar database returns a total of 10 m⁶A variants identified in two lung cancer types. The details of which can be viewed by clicking the m6A-CAVar ID. **B.** Users can further filter the search results in specific cancer types. **C.** A human body map provided on the front page of m6A-CAVar website. It enables quick positioning of cancer m⁶A-associated variants functioning at a specific tissue. **D.** The disease and phenotype associations of recorded m⁶A variant.

m⁶A writer METTL3 regulates *EGFR* expression to promote cell invasion of human lung cancer cells [82]. The m6A-CAVar database can be used to explore the role of m⁶A variants of *EGFR* in lung cancers. We first search by gene name '*EGFR*' on the front page of the m6A-CAVar database, then filter the results and keep only records related to lung tissue, which retains a total of 10 cancer m⁶A-associated variants from two lung cancer types (Figure 6A and B). Alternatively, the users can query all recorded m⁶A-associated variants that function in lung tissue by simply clicking the relevant part from the human body diagram (Figure 6C). More details can be accessed by clicking the variant ID. For example, if we check further details of an m⁶A-gain variant from the TCGA-LUAD project at Chr7:55259515 (T > G), we can see that this variant is recorded in the ClinVar database and is relevant to eight disease conditions, including lung cancers (Figure 6D), which may suggest potential cancer pathogenesis originates in the epitranscriptome layer.

Discussion and perspectives

The context-specific expression and functions of m⁶A regulators have been repeatedly reported in existing studies [59–63], suggesting the involvement of the tissue-specific m⁶A methylome in essential biological processes and multiple disease mechanisms. Besides, the associations between RNA methylation levels and the activities of RNA methylation

regulators were clearly unveiled, reporting that there exist some condition-specific RNA co-methylation patterns (a group of RNA m⁶A methylation sites whose methylation levels go up and down together) [108–110]. These co-methylation patterns are enriched by the substrate targets of m⁶A regulators and thus are probably regulated by specific m⁶A methyltransferase or demethylase.

Here, we present m6A-TSHub, a comprehensive online platform for unveiling the context-specific m⁶A methylation and m⁶A-affecting mutations in 23 human tissues and 25 tumor conditions. In m6A-TSHub, a total of 184,554 and 499,369 m⁶A sites derived from 23 normal human tissues and 25 matched tumor samples were collected (m6A-TSDB), from which some potential patterns for the tissue-specific m⁶A modification sites were revealed (e.g., heart-enriched genes *RYS2* and *PXDNL*; Figure S2). Based on these collected data, 23 distinct m⁶A prediction models were built at the tissue level using deep neural networks (m6A-TSfinder). In addition, to elucidate the genetic factor of epitranscriptome dysregulation, m6A-CAVar identified a total of 587,983 cancer somatic mutations that may alter the m⁶A status in corresponding cancer originating tissues and annotated them with various functional annotations, including features relating to post-transcriptional regulations (RBP binding regions, miRNA targets, and splicing sites), disease and phenotype associations, as well as other useful genomic information (transcript structure, phastCons, and deleterious level) to provide a more comprehensive overview. We also provide a web server m6A-TSVar

for assessing the effect of genetic variants on m⁶A methylation in a specific tissue.

Although most of the existing approaches for RNA modification site prediction ignore the tissue-specific signatures of m⁶A methylation, by taking advantage of existing tissue-specific epitranscriptome data, our method can predict the m⁶A methylation within a specific tissue. Compared with existing approaches for tissue-specific m⁶A methylation site prediction [64–66], our approach m6A-TSFinder achieved a higher prediction performance (Table 2) and hugely expanded the number of supported tissue types from 3 to 23 (Table 1).

Compared with existing approaches for decoding the epitranscriptome impact of genetic variants, m6A-CAVar has the following two major advantages. First, m6A-CAVar relies on a finer prediction model (m6A-TSFinder) that appreciates the specific pattern of RNA methylomes across different tissues. By directly learning from the epitranscriptome profiles in 23 healthy human tissues, m6A-CAVar is able to evaluate the tissue-specific impact of cancer somatic variants on m⁶A modification in their originating tissue, providing a more detailed picture of the genome–epitranscriptome association. This improves on existing approaches that ignore the distinct signatures of RNA methylation across different tissues and thus fail to address tissue-specific effects. Second, the predicted m⁶A dynamics in m6A-CAVar were systematically validated using available epitranscriptome datasets from the matched healthy and cancerous samples, providing another layer of quality assurance from real omic datasets. In contrast, existing approaches use those datasets only to provide the m⁶A site information without searching for potential evidence of m⁶A status switching.

To date, epitranscriptome data are still rather scarce. Due to the limited availability of datasets, matched healthy tissue and cancer m⁶A profiling samples are only available for 14 out of the total 27 cancer types, prohibiting a more thorough validation of the predicted results. Furthermore, a substantial discrepancy has been observed among different RNA modification profiling approaches due to technical biases [111–114], which can produce additional inaccuracy. Currently, context-specific epitranscriptome prediction is only possible for a small number of conditions (cell line, tissue type, and treatment) with data [64–66]. However, the m6A-TSFinder framework will be further expanded when epitranscriptome datasets are more abundantly available for more comprehensive and less biased screening of context-specific m⁶A-variants, along with linking the tissue-specific epitranscriptome patterns with other important cancer-associated factors such as human aging [67,115]. Besides, the current version of m6A-TSFinder was built on human genome assemble hg19. A LiftOver file from hg19 to hg38 was provided on the ‘download’ page, and the next version of the database will be updated based on the latest genome assembly. Particularly promising is the recent development in Nanopore direct RNA sequencing technology that enables simultaneous identification of multiple RNA modifications with simplified sample preparation procedures [116–124].

Data availability

The data underlying this article are available at www.xjtlu.edu.cn/biologicalsciences/m6ats. The online versions of the

m6A-TSFinder and m6A-TSVar web server are available at www.xjtlu.edu.cn/biologicalsciences/m6ats by clicking the ‘tool’ section. The local version and project codes can be accessed on the ‘download’ page.

Competing interests

The authors declare that they have no competing interests.

CRediT authorship contribution statement

Bowen Song: Methodology, Data curation, Software, Visualization, Writing – original draft. **Daiyun Huang:** Software, Supervision. **Yuxin Zhang:** Visualization. **Zhen Wei:** Resources. **Jionglong Su:** Visualization. **João Pedro de Magalhães:** Visualization. **Daniel J. Rigden:** Writing – review & editing. **Jia Meng:** Conceptualization, Supervision, Writing – review & editing, Funding acquisition. **Kunqi Chen:** Conceptualization, Resources, Writing – review & editing, Funding acquisition. All authors have read and approved the final manuscript.

Acknowledgments

This work was supported by the National Natural Science Foundation of China (Grant Nos. 32100519 and 31671373), the Scientific Research Foundation for Advanced Talents of Fujian Medical University (Grant No. XRCZX2021019), and the XJTLU Key Program Special Fund (Grant Nos. KSF-T-01, KSF-E-51, and KSF-P-02), China. The authors also acknowledge the researcher of the various resources mentioned in the manuscript to share their data, especially for tissue-specific m⁶A sequencing data.

Supplementary material

Supplementary data to this article can be found online at <https://doi.org/10.1016/j.gpb.2022.09.001>.

ORCID

ORCID 0000-0002-8586-0573 (Bowen Song)
ORCID 0000-0002-3067-7165 (Daiyun Huang)
ORCID 0000-0003-1900-6712 (Yuxin Zhang)
ORCID 0000-0002-1614-9614 (Zhen Wei)
ORCID 0000-0001-5360-6493 (Jionglong Su)
ORCID 0000-0002-6363-2465 (João Pedro de Magalhães)
ORCID 0000-0002-7565-8937 (Daniel J. Rigden)
ORCID 0000-0003-3455-205X (Jia Meng)
ORCID 0000-0002-6025-8957 (Kunqi Chen)

References

- [1] Boccaletto P, Machnicka MA, Purta E, Piatkowski P, Baginski B, Wirecki TK, et al. MODOMICS: a database of RNA modification pathways. 2017 update. *Nucleic Acids Res* 2018;46:D303–7.

- [2] Meyer KD, Jaffrey SR. Rethinking m⁶A readers, writers, and erasers. *Annu Rev Cell Dev Biol* 2017;33:319–42.
- [3] Niu Y, Zhao X, Wu YS, Li MM, Wang XJ, Yang YG. N⁶-methyl-adenosine (m⁶A) in RNA: an old modification with a novel epigenetic function. *Genomics Proteomics Bioinformatics* 2013;11:8–17.
- [4] Wang X, Lu Z, Gomez A, Hon GC, Yue Y, Han D, et al. N⁶-methyladenosine-dependent regulation of messenger RNA stability. *Nature* 2014;505:117–20.
- [5] Mendel M, Delaney K, Pandey RR, Chen KM, Wenda JM, Vågbo CB, et al. Splice site m⁶A methylation prevents binding of U2AF35 to inhibit RNA splicing. *Cell* 2021;184:3125–42.e25.
- [6] Choe J, Lin S, Zhang W, Liu Q, Wang L, Ramirez-Moya J, et al. mRNA circularization by METTL3-eIF3h enhances translation and promotes oncogenesis. *Nature* 2018;561:556–60.
- [7] Barbieri I, Tzelepis K, Pandolfini L, Shi J, Millan-Zambrano G, Robson SC, et al. Promoter-bound METTL3 maintains myeloid leukaemia by m⁶A-dependent translation control. *Nature* 2017;552:126–31.
- [8] Zhou J, Wan J, Gao X, Zhang X, Jaffrey SR, Qian SB. Dynamic m⁶A mRNA methylation directs translational control of heat shock response. *Nature* 2015;526:591–4.
- [9] Xiang Y, Laurent B, Hsu CH, Nachtergaele S, Lu Z, Sheng W, et al. RNA m⁶A methylation regulates the ultraviolet-induced DNA damage response. *Nature* 2017;543:573–6.
- [10] Zhong S, Li H, Bodi Z, Button J, Vespa L, Herzog M, et al. MTA is an *Arabidopsis* messenger RNA adenosine methylase and interacts with a homolog of a sex-specific splicing factor. *Plant Cell* 2008;20:1278–88.
- [11] Zhou Y, Zeng P, Li YH, Zhang Z, Cui Q. SRAMP: prediction of mammalian N⁶-methyladenosine (m⁶A) sites based on sequence-derived features. *Nucleic Acids Res* 2016;44:e91.
- [12] Zhang C, Zhi WI, Lu H, Samanta D, Chen I, Gabrielson E, et al. Hypoxia-inducible factors regulate pluripotency factor expression by ZNF217- and ALKBH5-mediated modulation of RNA methylation in breast cancer cells. *Oncotarget* 2016;7:64527–42.
- [13] Lewis SJ, Murad A, Chen L, Davey Smith G, Donovan J, Palmer T, et al. Associations between an obesity related genetic variant (FTO rs9939609) and prostate cancer risk. *PLoS One* 2010;5:e13485.
- [14] Yankova E, Blackaby W, Albertella M, Rak J, De Braekeleer E, Tsagkogeorga G, et al. Small molecule inhibition of METTL3 as a strategy against myeloid leukaemia. *Nature* 2021;593:597–601.
- [15] Dominissini D, Moshitch-Moshkovitz S, Schwartz S, Salmon-Divon M, Ungar L, Osenberg S, et al. Topology of the human and mouse m⁶A RNA methylomes revealed by m⁶A-seq. *Nature* 2012;485:201–6.
- [16] Meyer KD, Saletore Y, Zumbo P, Elemento O, Mason CE, Jaffrey SR. Comprehensive analysis of mRNA methylation reveals enrichment in 3' UTRs and near stop codons. *Cell* 2012;149:1635–46.
- [17] Linder B, Grozhik AV, Olarerin-George AO, Meydan C, Mason CE, Jaffrey SR. Single-nucleotide-resolution mapping of m⁶A and m⁶Am throughout the transcriptome. *Nat Methods* 2015;12:767–72.
- [18] Ke S, Pandya-Jones A, Saito Y, Fak JJ, Vagbo CB, Geula S, et al. m⁶A mRNA modifications are deposited in nascent pre-mRNA and are not required for splicing but do specify cytoplasmic turnover. *Genes Dev* 2017;31:990–1006.
- [19] Zhang Z, Chen LQ, Zhao YL, Yang CG, Roundtree IA, Zhang Z, et al. Single-base mapping of m⁶A by an antibody-independent method. *Sci Adv* 2019;5:eaax0250.
- [20] Meyer KD. DART-seq: an antibody-free method for global m⁶A detection. *Nat Methods* 2019;16:1275–80.
- [21] Liu L, Song B, Ma J, Song Y, Zhang SY, Tang Y, et al. Bioinformatics approaches for deciphering the epitranscriptome: recent progress and emerging topics. *Comput Struct Biotechnol J* 2020;18:1587–604.
- [22] Chen Z, Zhao P, Li F, Wang Y, Smith AI, Webb GI, et al. Comprehensive review and assessment of computational methods for predicting RNA post-transcriptional modification sites from RNA sequences. *Brief Bioinform* 2020;21:1676–96.
- [23] Qiu WR, Jiang SY, Sun BQ, Xiao X, Cheng X, Chou KC. iRNA-2methyl: identify RNA 2'-O-methylation sites by incorporating sequence-coupled effects into general PseKNC and Ensemble classifier. *Med Chem* 2017;13:734–43.
- [24] Yang H, Lv H, Ding H, Chen W, Lin H. iRNA-2OM: a sequence-based predictor for identifying 2'-O-methylation sites in *Homo sapiens*. *J Comput Biol* 2018;25:1266–77.
- [25] Chen W, Ding H, Zhou X, Lin H, Chou KC. iRNA(m6A)-PseDNC: identifying N⁶-methyladenosine sites using pseudo dinucleotide composition. *Anal Biochem* 2018;561–62:59–65.
- [26] Chen W, Feng P, Ding H, Lin H, Chou KC. iRNA-Methyl: identifying N⁶-methyladenosine sites using pseudo nucleotide composition. *Anal Biochem* 2015;490:26–33.
- [27] Qiu WR, Jiang SY, Xu ZC, Xiao X, Chou KC. iRNAm5C-PseDNC: identifying RNA 5-methylcytosine sites by incorporating physical-chemical properties into pseudo dinucleotide composition. *Oncotarget* 2017;8:41178–88.
- [28] Chen W, Song X, Lv H, Lin H. iRNA-m2G: identifying N²-methylguanosine sites based on sequence-derived information. *Mol Ther Nucleic Acids* 2019;18:253–8.
- [29] Chen W, Feng P, Song X, Lv H, Lin H. iRNA-m7G: identifying N⁷-methylguanosine sites by fusing multiple features. *Mol Ther Nucleic Acids* 2019;18:269–74.
- [30] Tahir M, Tayara H, Chong KT. iRNA-PseKNC(2methyl): identify RNA 2'-O-methylation sites by convolution neural network and Chou's pseudo components. *J Theor Biol* 2019;465:1–6.
- [31] Chen W, Tang H, Ye J, Lin H, Chou KC. iRNA-PseU: identifying RNA pseudouridine sites. *Mol Ther Nucleic Acids* 2016;5:e332.
- [32] Song Z, Huang D, Song B, Chen K, Song Y, Liu G, et al. Attention-based multi-label neural networks for integrated prediction and interpretation of twelve widely occurring RNA modifications. *Nat Commun* 2021;12:4011.
- [33] Fang T, Zhang Z, Sun R, Zhu L, He J, Huang B, et al. RNAm5CPred: prediction of RNA 5-methylcytosine sites based on three different kinds of nucleotide composition. *Mol Ther Nucleic Acids* 2019;18:739–47.
- [34] Zou Q, Xing P, Wei L, Liu B. Gene2vec: gene subsequence embedding for prediction of mammalian N⁶-methyladenosine sites from mRNA. *RNA* 2019;25:205–18.
- [35] Zhai J, Song J, Cheng Q, Tang Y, Ma C. PEA: an integrated R toolkit for plant epitranscriptome analysis. *Bioinformatics* 2018;34:3747–9.
- [36] Li YH, Zhang G, Cui Q. PPUS: a web server to predict PUS-specific pseudouridine sites. *Bioinformatics* 2015;31:3362–4.
- [37] Chen K, Wei Z, Zhang Q, Wu X, Rong R, Lu Z, et al. WHISTLE: a high-accuracy map of the human N⁶-methyladenosine (m⁶A) epitranscriptome predicted using a machine learning approach. *Nucleic Acids Res* 2019;47:e41.
- [38] Jiang J, Song B, Tang Y, Chen K, Wei Z, Meng J. m5UPred: a web server for the prediction of RNA 5-methyluridine sites from sequences. *Mol Ther Nucleic Acids* 2020;22:742–7.
- [39] Huang D, Song B, Wei J, Su J, Coenen F, Meng J. Weakly supervised learning of RNA modifications from low-resolution epitranscriptome data. *Bioinformatics* 2021;37:i222–30.
- [40] Liang Z, Zhang L, Chen H, Huang D, Song B. m6A-Maize: weakly supervised prediction of m⁶A-carrying transcripts and m⁶A-affecting mutations in maize (*Zea mays*). *Methods* 2022;203:226–32.
- [41] Körte N, Rücklé C, Zhou Y, Busch A, Hoch-Kraft P, Sutandy FXR, et al. Deep and accurate detection of m⁶A RNA modifications using miCLIP2 and m6Aboost machine learning. *Nucleic Acids Res* 2021;49:e92.

- [42] He X, Zhang S, Zhang Y, Lei Z, Jiang T, Zeng J. Characterizing RNA pseudouridylation by convolutional neural networks. *Genomics Proteomics Bioinformatics* 2021;19:815–33.
- [43] Chen Z, Zhao P, Li C, Li F, Xiang D, Akutsu T, et al. iLearnPlus: a comprehensive and automated machine-learning platform for nucleic acid and protein sequence analysis, prediction and visualization. *Nucleic Acids Res* 2021;49:e60.
- [44] Huang Y, He N, Chen Y, Chen Z, Li L. BERMP: a cross-species classifier for predicting m⁶A sites by integrating a deep learning algorithm and a random forest approach. *Int J Biol Sci* 2018;14:1669–77.
- [45] Xiong Y, He X, Zhao D, Tian T, Hong L, Jiang T, et al. Modeling multi-species RNA modification through multi-task curriculum learning. *Nucleic Acids Res* 2021;49:3719–34.
- [46] Zhu X, He J, Zhao S, Tao W, Xiong Y, Bi S. A comprehensive comparison and analysis of computational predictors for RNA N⁶-methyladenosine sites of *Saccharomyces cerevisiae*. *Brief Funct Genomics* 2019;18:367–76.
- [47] Lv H, Zhang ZM, Li SH, Tan JX, Chen W, Lin H. Evaluation of different computational methods on 5-methylcytosine sites identification. *Brief Bioinform* 2019;21:982–95.
- [48] Chen X, Sun YZ, Liu H, Zhang L, Li JQ, Meng J. RNA methylation and diseases: experimental results, databases, web servers and computational models. *Brief Bioinform* 2019;20:896–917.
- [49] Xuan JJ, Sun WJ, Lin PH, Zhou KR, Liu S, Zheng LL, et al. RMBase v2.0: deciphering the map of RNA modifications from epitranscriptome sequencing data. *Nucleic Acids Res* 2018;46:D327–34.
- [50] Ma J, Song B, Wei Z, Huang D, Zhang Y, Su J, et al. m⁵C-Atlas: a comprehensive database for decoding and annotating the 5-methylcytosine (m⁵C) epitranscriptome. *Nucleic Acids Res* 2022;50:D196–203.
- [51] Tang Y, Chen K, Song B, Ma J, Wu X, Xu Q, et al. m⁶A-Atlas: a comprehensive knowledgebase for unraveling the N⁶-methyladenosine (m⁶A) epitranscriptome. *Nucleic Acids Res* 2020;49:D134–43.
- [52] Liu S, Zhu A, He C, Chen M. REPIC: a database for exploring the N⁶-methyladenosine methylome. *Genome Biol* 2020;21:100.
- [53] Song B, Chen K, Tang Y, Wei Z, Su J, Magalhães JP, et al. ConsRM: collection and large-scale prediction of the evolutionarily conserved RNA methylation sites, with implications for the functional epitranscriptome. *Brief Bioinform* 2021;22:1–17.
- [54] Deng S, Zhang H, Zhu K, Li X, Ye Y, Li R, et al. M6A2Target: a comprehensive database for targets of m⁶A writers, erasers and readers. *Brief Bioinform* 2020;22:1–11.
- [55] Zheng Y, Nie P, Peng D, He Z, Liu M, Xie Y, et al. m6AVar: a database of functional variants involved in m⁶A modification. *Nucleic Acids Res* 2018;46:D139–45.
- [56] Luo X, Li H, Liang J, Zhao Q, Xie Y, Ren J, et al. RMVar: an updated database of functional variants involved in RNA modifications. *Nucleic Acids Res* 2021;49:D1405–12.
- [57] Chen K, Song B, Tang Y, Wei Z, Su J, Meng J. RMDisease: a database of genetic variants that affect RNA modifications, with implications for epitranscriptome pathogenesis. *Nucleic Acids Res* 2020;49:D1396–404.
- [58] Ma J, Zhang L, Chen S, Liu H. A brief review of RNA modification related database resources. *Methods* 2022;203:342–53.
- [59] Begik O, Lucas MC, Liu H, Ramirez JM, Mattick JS, Novoa EM. Integrative analyses of the RNA modification machinery reveal tissue- and cancer-specific signatures. *Genome Biol* 2020;21:97.
- [60] Zhang H, Shi X, Huang T, Zhao X, Chen W, Gu N, et al. Dynamic landscape and evolution of m⁶A methylation in human. *Nucleic Acids Res* 2020;48:6251–64.
- [61] Liu J, Li K, Cai J, Zhang M, Zhang X, Xiong X, et al. Landscape and regulation of m⁶A and m⁶Am methylome across human and mouse tissues. *Mol Cell* 2020;77:426–40.e6.
- [62] An S, Huang W, Huang X, Cun Y, Cheng W, Sun X, et al. Integrative network analysis identifies cell-specific *trans* regulators of m⁶A. *Nucleic Acids Res* 2020;48:1715–29.
- [63] Xiong X, Hou L, Park YP, Molinie B, Gregory RI, Kellis M. Genetic drivers of m⁶A methylation in human brain, lung, heart and muscle. *Nat Genet* 2021;53:1–10.
- [64] Liu K, Cao L, Du P, Chen W. im6A-TS-CNN: identifying the N⁶-methyladenine site in multiple tissues by using the convolutional neural network. *Mol Ther Nucleic Acids* 2020;21:1044–9.
- [65] Dao FY, Lv H, Yang YH, Zulfiqar H, Gao H, Lin H. Computational identification of N⁶-methyladenosine sites in multiple tissues of mammals. *Comput Struct Biotechnol J* 2020;18:1084–91.
- [66] Abbas Z, Tayara H, Zou Q, Chong KT. TS-m6A-DL: tissue-specific identification of N⁶-methyladenosine sites using a universal deep learning model. *Comput Struct Biotechnol J* 2021;19:4619–25.
- [67] Chatsirisupachai K, Lesluyes T, Paraoan L, Van Loo P, de Magalhães JP. An integrative analysis of the age-associated multi-omic landscape across cancers. *Nat Commun* 2021;12:2345.
- [68] Silva AS, Wood SH, van Dam S, Berres S, McArdle A, de Magalhães JP. Gathering insights on disease etiology from gene expression profiles of healthy tissues. *Bioinformatics* 2011;27:3300–5.
- [69] Pei G, Hu R, Jia P, Zhao Z. DeepFun: a deep learning sequence-based model to decipher non-coding variant effect in a tissue- and cell type-specific manner. *Nucleic Acids Res* 2021;49:W131–9.
- [70] Buniello A, MacArthur JAL, Cerezo M, Harris LW, Hayhurst J, Malangone C, et al. The NHGRI-EBI GWAS catalog of published genome-wide association studies, targeted arrays and summary statistics 2019. *Nucleic Acids Res* 2018;47:D1005–12.
- [71] Landrum MJ, Lee JM, Benson M, Brown G, Chao C, Chitipiralla S, et al. ClinVar: public archive of interpretations of clinically relevant variants. *Nucleic Acids Res* 2015;44:D862–8.
- [72] Wheeler DL, Church DM, Edgar R, Federhen S, Helmberg W, Madden TL, et al. Database resources of the national center for biotechnology information. *Nucleic Acids Res* 2004;32:13–6.
- [73] CNCB-NGDC Members and Partners. Database Resources of the National Genomics Data Center, China National Center for Bioinformation in 2021. *Nucleic Acids Res* 2021;49:D18–28.
- [74] Martin M. Cutadapt removes adapter sequences from high-throughput sequencing reads. *EMBnet J* 2011;17:10–2.
- [75] Kim D, Paggi JM, Park C, Bennett C, Salzberg SL. Graph-based genome alignment and genotyping with HISAT2 and HISAT-genotype. *Nat Biotechnol* 2019;37:907–15.
- [76] Meng J, Lu Z, Liu H, Zhang L, Zhang S, Chen Y, et al. A protocol for RNA methylation differential analysis with MeRIP-seq data and exomePeak R/Bioconductor package. *Methods* 2014;69:274–81.
- [77] Tomczak K, Czerwińska P, Wiznerowicz M. The Cancer Genome Atlas (TCGA): an immeasurable source of knowledge. *Contemp Oncol* 2015;19:A68.
- [78] Huang D, Song B, Wei J, Su J, Coenen F, Meng J. Weakly supervised learning of RNA modifications from low-resolution epitranscriptome data. *Bioinformatics* 2021;37:i222–30.
- [79] Song B, Tang Y, Chen K, Wei Z, Rong R, Lu Z, et al. m7GHub: deciphering the location, regulation and pathogenesis of internal mRNA N⁷-methylguanosine (m⁷G) sites in human. *Bioinformatics* 2020;36:3528–36.
- [80] Sun WJ, Li JH, Liu S, Wu J, Zhou H, Qu LH, et al. RMBase: a resource for decoding the landscape of RNA modifications from

- high-throughput sequencing data. *Nucleic Acids Res* 2016;44:D259–65.
- [81] Schwartz S, Mumbach MR, Jovanovic M, Wang T, Maciag K, Bushkin GG, et al. Perturbation of m⁶A writers reveals two distinct classes of mRNA methylation at internal and 5' sites. *Cell Rep* 2014;8:284–96.
- [82] Lin S, Choe J, Du P, Triboulet R, Gregory RI. The m⁶A methyltransferase METTL3 promotes translation in human cancer cells. *Mol Cell* 2016;62:335–45.
- [83] Kumar P, Henikoff S, Ng PC. Predicting the effects of coding non-synonymous variants on protein function using the SIFT algorithm. *Nat Protoc* 2009;4:1073–81.
- [84] Adzhubei IA, Schmidt S, Peshkin L, Ramensky VE, Gerasimova A, Bork P, et al. A method and server for predicting damaging missense mutations. *Nat Methods* 2010;7:248–9.
- [85] Chun S, Fay JC. Identification of deleterious mutations within three human genomes. *Genome Res* 2009;19:1553–61.
- [86] Shihab HA, Gough J, Cooper DN, Stenson PD, Barker GL, Edwards KJ, et al. Predicting the functional, molecular, and phenotypic consequences of amino acid substitutions using hidden Markov models. *Hum Mutat* 2013;34:57–65.
- [87] Wang K, Li M, Hakonarson H. ANNOVAR: functional annotation of genetic variants from high-throughput sequencing data. *Nucleic Acids Res* 2010;38:e164.
- [88] Zhu Y, Xu G, Yang YT, Xu Z, Chen X, Shi B, et al. POSTAR2: deciphering the post-transcriptional regulatory logics. *Nucleic Acids Res* 2018;47:D203–11.
- [89] Agarwal V, Bell GW, Nam JW, Bartel DP. Predicting effective microRNA target sites in mammalian mRNAs. *Elife* 2015;4:e05005.
- [90] Li JH, Liu S, Zhou H, Qu LH, Yang JH. starBase v2.0: decoding miRNA–ceRNA, miRNA–ncRNA and protein–RNA interaction networks from large-scale CLIP-seq data. *Nucleic Acids Res* 2013;42:D92–7.
- [91] Lawrence M, Huber W, Pages H, Aboyoun P, Carlson M, Gentleman R, et al. Software for computing and annotating genomic ranges. *PLoS Comput Biol* 2013;9:e1003118.
- [92] Buels R, Yao E, Diesh CM, Hayes RD, Holmes IH. JBrowse: a dynamic web platform for genome visualization and analysis. *Genome Biol* 2016;17:66.
- [93] Zhang SY, Zhang SW, Zhang T, Fan XN, Meng J. Recent advances in functional annotation and prediction of the epitranscriptome. *Comput Struct Biotechnol J* 2021;19:3015–26.
- [94] Zhang S, Zhao BS, Zhou A, Lin K, Zheng S, Lu Z, et al. m⁶A demethylase ALKBH5 maintains tumorigenicity of glioblastoma stem-like cells by sustaining FOXM1 expression and cell proliferation program. *Cancer Cell* 2017;31:591–606.e6.
- [95] Hou YY, Cao WW, Li L, Li SP, Liu T, Wan HY, et al. MicroRNA-519d targets *MKI67* and suppresses cell growth in the hepatocellular carcinoma cell line QGY-7703. *Cancer Lett* 2011;307:182–90.
- [96] Geng Y, Guan R, Hong W, Huang B, Liu P, Guo X, et al. Identification of m⁶A-related genes and m⁶A RNA methylation regulators in pancreatic cancer and their association with survival. *Ann Transl Med* 2020;8:387.
- [97] Tate JG, Bamford S, Jubb HC, Sondka Z, Beare DM, Bindal N, et al. COSMIC: the catalogue of somatic mutations in cancer. *Nucleic Acids Res* 2019;47:D941–7.
- [98] Liu T, Li C, Jin L, Li C, Wang L. The prognostic value of m⁶A RNA methylation regulators in colon adenocarcinoma. *Med Sci Monit* 2019;25:9435–45.
- [99] Yang Z, Wang T, Wu D, Min Z, Tan J, Yu B. RNA N⁶-methyladenosine reader IGF2BP3 regulates cell cycle and angiogenesis in colon cancer. *J Exp Clin Cancer Res* 2020;39:203.
- [100] Guo T, Liu DF, Peng SH, Xu AM. ALKBH5 promotes colon cancer progression by decreasing methylation of the lncRNA NEAT1. *Am J Transl Res* 2020;12:4542–9.
- [101] Ni W, Yao S, Zhou Y, Liu Y, Huang P, Zhou A, et al. Long noncoding RNA GAS5 inhibits progression of colorectal cancer by interacting with and triggering YAP phosphorylation and degradation and is negatively regulated by the m⁶A reader YTHDF3. *Mol Cancer* 2019;18:143.
- [102] Kim SH, Joshi K, Ezhilarasan R, Myers TR, Siu J, Gu C, et al. EZH2 protects glioma stem cells from radiation-induced cell death in a MELK/FOXM1-dependent manner. *Stem Cell Rep* 2015;4:226–38.
- [103] Schonberg DL, Miller TE, Wu Q, Flavahan WA, Das NK, Hale JS, et al. Preferential iron trafficking characterizes glioblastoma stem-like cells. *Cancer Cell* 2015;28:441–55.
- [104] Zhang N, Wei P, Gong A, Chiu WT, Lee HT, Colman H, et al. FoxM1 promotes β -catenin nuclear localization and controls Wnt target-gene expression and glioma tumorigenesis. *Cancer Cell* 2011;20:427–42.
- [105] Li Y, Zhang S, Huang S. FoxM1: a potential drug target for glioma. *Future Oncol* 2012;8:223–6.
- [106] Yarmishyn AA, Yang YP, Lu KH, Chen YC, Chien Y, Chou SJ, et al. Musashi-1 promotes cancer stem cell properties of glioblastoma cells via upregulation of YTHDF1. *Cancer Cell Int* 2020;20:1–15.
- [107] Liu J, Ren D, Du Z, Wang H, Zhang H, Jin Y. m⁶A demethylase FTO facilitates tumor progression in lung squamous cell carcinoma by regulating MZF1 expression. *Biochem Biophys Res Commun* 2018;502:456–64.
- [108] Liu L, Zhang SW, Zhang YC, Liu H, Zhang L, Chen R, et al. Decomposition of RNA methylome reveals co-methylation patterns induced by latent enzymatic regulators of the epitranscriptome. *Mol Biosyst* 2015;11:262–74.
- [109] Zhang L, Chen S, Ma J, Liu Z, Liu H. REW-ISA V2: a biclustering method fusing homologous information for analyzing and mining epi-transcriptome data. *Front Genet* 2021;12:654820.
- [110] Chen S, Zhang L, Lu L, Meng J, Liu H. FBCwPlaid: a functional bi-clustering analysis of epi-transcriptome profiling data via a weighted plaid model. *IEEE/ACM Trans Comput Biol Bioinform* 2022;19:1640–50.
- [111] Adachi H, De Zoysa MD, Yu YT. Post-transcriptional pseudouridylation in mRNA as well as in some major types of noncoding RNAs. *Biochim Biophys Acta Gene Regul Mech* 2019;1862:230–9.
- [112] Zaringhalam M, Papavasiliou FN. Pseudouridylation meets next-generation sequencing. *Methods* 2016;107:63–72.
- [113] Hussain S, Aleksic J, Blanco S, Dietmann S, Frye M. Characterizing 5-methylcytosine in the mammalian epitranscriptome. *Genome Biol* 2013;14:215.
- [114] Capitanchik C, Toolan-Kerr P, Luscombe NM, Ule J. How do you identify m⁶A methylation in transcriptomes at high resolution? A comparison of recent datasets. *Front Genet* 2020;11:398.
- [115] Chatsirisupachai K, Palmer D, Ferreira S, de Magalhaes JP. A human tissue-specific transcriptomic analysis reveals a complex relationship between aging, cancer, and cellular senescence. *Aging Cell* 2019;18:e13041.
- [116] Gao Y, Liu X, Wu B, Wang H, Xi F, Kohnen MV, et al. Quantitative profiling of N⁶-methyladenosine at single-base resolution in stem-differentiating xylem of *Populus trichocarpa* using nanopore direct RNA sequencing. *Genome Biol* 2021;22:22.
- [117] Smith MA, Ersavas T, Ferguson JM, Liu H, Lucas MC, Begik O, et al. Molecular barcoding of native RNAs using nanopore sequencing and deep learning. *Genome Res* 2020;30:1345–53.
- [118] Viehweger A, Krautwurst S, Lamkiewicz K, Madhugiri R, Ziebuhr J, Holzer M, et al. Direct RNA nanopore sequencing of full-length coronavirus genomes provides novel insights into structural variants and enables modification analysis. *Genome Res* 2019;29:1545–54.

- [119] Begik O, Lucas MC, Prysycz LP, Ramirez JM, Medina R, Milenkovic I, et al. Quantitative profiling of pseudouridylation dynamics in native RNAs with nanopore sequencing. *Nat Biotechnol* 2021;39:1278–91.
- [120] Liu H, Begik O, Lucas MC, Ramirez JM, Mason CE, Wiener D, et al. Accurate detection of m⁶A RNA modifications in native RNA sequences. *Nat Commun* 2019;10:4079.
- [121] McIntyre ABR, Alexander N, Grigorev K, Bezdan D, Sichtig H, Chiu CY, et al. Single-molecule sequencing detection of N⁶-methyladenine in microbial reference materials. *Nat Commun* 2019;10:579.
- [122] Price AM, Hayer KE, McIntyre ABR, Gokhale NS, Abebe JS, Della Fera AN, et al. Direct RNA sequencing reveals m⁶A modifications on adenovirus RNA are necessary for efficient splicing. *Nat Commun* 2020;11:6016.
- [123] Prysycz LP, Novoa EM. ModPhred: an integrative toolkit for the analysis and storage of nanopore sequencing DNA and RNA modification data. *Bioinformatics* 2021;38:257–60.
- [124] Pratanwanich PN, Yao F, Chen Y, Koh CWQ, Wan YK, Hendra C, et al. Identification of differential RNA modifications from nanopore direct RNA sequencing with xPore. *Nat Biotechnol* 2021;39:1394–402.